Modeling for Collapsing Cavitation Bubble near Rough Solid Wall by Mulit-Relaxation-Time Pseudopotential Lattice Boltzmann Model

Minglei Shan[1,2], Yipeng Zhu[1], Cheng Yao[1,2], Qingbang Han[1,2], Changping Zhu[1,2]

[1]College of Internet of Things Engineering, Hohai University, Changzhou, China
[2]Jiangsu Key Laboratory of Power Transmission and Distribution Equipment Technology, Hohai University, Changzhou, China
Email: shanming2003@126.com

Abstract

Cavitation bubble collapse near rough solid wall is modeled by the multi-relaxation-time (MRT) pseudopotential lattice Boltzmann (LB) model. The modified forcing scheme, which can achieve LB model's thermodynamic consistency by tuning a parameter related with the particle interaction range, is adopted to achieve desired stability and density ratio. The bubble collapse near rough solid wall was simulated by the improved MRT pseudopotential LB model. The mechanism of bubble collapse is studied by investigating the bubble profiles, pressure field and velocity field evolution. The eroding effects of collapsing bubble are analyzed in details. It is found that the process and the effect of the interaction between bubble collapse and rough solid wall are affected seriously by the geometry of solid boundary. At the same time, it demonstrates that the MRT pseudopotential LB model is a potential tool for the investigation of the interaction mechanism between the collapsing bubble and complex geometry boundary.

Keywords

Cavitation Bubble, Bubble Collapse, Lattice Boltzmann Method, Pseudopotential Model, Rough Solid Wall

1. Introduction

Cavitation is ubiquitous in liquid, and happens when the local pressure is below the saturated vapor pressure. As cavitation bubble collapse near a solid wall, the associated phenomena include instant high pressure, high velocity jets and high temperature, which closely relate with the cavitation erosion of the solid material surface. On the other side, the collapse of the cavitation bubble has been applied

in environmental protection, ultrasonic therapy, lab on chip and material surface cleaning [1] [2].

The mechanism of the cavitation bubble collapse near solid wall is a fundamental issue for the above applications. However, as too many phenomena are involved, theoretical model of cavitation bubble collapse is difficult to be established, and for complex geometry boundary, the analytical solution is even impossible. Many publications are devoted to the investigation of the bubble collapse near the planar wall starting from the experimental work [3]. In recent years, many works have been developed to investigate the interaction between collapsing bubble and non-planar solid wall [1] [4], and numerical methods are becoming more and more important tools to study the bubble collapse near solid wall [5] [6]. Commonly used numerical methods include the finite volume method (FVM) [4], the finite element method (FEM) [7], and the boundary element method (BEM) [8]. These macroscopic numerical modeling methods based on solving partial differential equations are limited in processing the multiphase flows and complex geometry boundary conditions. As describing the multiphase flow, macroscopic methods need the assistance of the schemes of the interface tracking or capturing, which will reduce the computational efficiency. For the complex geometry boundary, it is difficult and inefficient to implement by macroscopic methods.

Owing to the flexibility for complex geometry boundary and the simplicity of the algorithm, the lattice Boltzmann method (LBM) has been developed into a powerful tool for the flow, heat and mass transfer simulations relating with complex geometry boundary [9] [10]. In LBM community, many multiphase models have been presented, which can be generally classified as the color-gradient model [11], the pseudopotential model (or Shan-Chen model) [12] [13], the free-energy model [14] and the phase-field model. The pseudopotential model is widely and successfully used in the LBM multiphase community due to its conceptual simplicity and computation efficiency [15] [16]. In the pseudopotential model, the fluid interactions are mimicked by an interparticle potential, from which a non-monotomic equation of state (EOS) can be obtained. As a result, the separation of fluid phases or components can be achieved automatically in this method, and the methods to track or capture the interfaces are not required.

In recent years, the pseudopotential model, as the top choice of the multiphase LB model, was introduced into the issue of cavitation by Sukop and Or [17]. Subsequently, several research efforts emerged to investigate the mechanism of cavitation. Chen [18] simulated the cavitation bubble growth using the modified pseudopotential LB model with the exact difference method (EDM) force scheme. The results in quiescent flows agree fairly well with the solution of Rayleigh- Plesset equation. Mishra [19] introduced a model of cavitation based on the pseudopotential LB model that allows for coupling between the hydrodynamics of a collapsing cavity and supported solute chemical species. Unfortunately, the above researches do not involve the interaction between bubble and solid wall. Until, the pseudopotential model was introduced into the researches

on the mechanism investigations of cavitation bubble collapse near solid wall by Shan *et al.* [20] [21]. However, these previous works involve just planar wall. In engineering cases, the rough walls are ubiquitous. The mechanism investigation of cavitation bubble collapse near rough wall is the basic issue for the efficient applications of cavitation bubble collapse.

One of the key challenges of the simulation of cavitation bubble collapse near rough wall is the stability of the LB model. For pseudopotential multiphase model, the stability is closely related to the thermodynamic consistency [22], and great efforts have been made for this issue [23] [24] [25]. Recently, Li *et al.* [24] [25] [26] founded that there exists a suitable forcing scheme, which can meet the thermodynamic consistency requirement in an efficient way. In order to investigate the interaction mechanism between the collapsing bubble and complex geometry boundary, in the present work, the improved forcing scheme for the pseudopotential MRT LB model developed by Li *et al.* [25] is adopted to achieve the sufficient density ratio and stability of the numerical model.

2. Numerical Method

The pseudopotential LB model, also well known as Shan-Chen model, was developed by Shan and Chen in 1993 [12]. In pseudopotential model, the fluid interactions are mimicked by an interparticle potential, which is now widely called pseudopotential. In original pseudopotential LB model, the Single-Relaxation-Time (SRT) collision operator was employed. In recent years, the MRT collision operator has been verified that it is superior to the SRT operator in terms of numerical stability. The MRT LB evolution equation can be given as follows:

$$f_\alpha \left(\boldsymbol{x} + \boldsymbol{e}_\alpha \delta_t, t + \delta_t \right) = f_\alpha \left(\boldsymbol{x}, t \right) - \left(\boldsymbol{M}^{-1} \boldsymbol{\Lambda} \boldsymbol{M} \right)_{\alpha\beta} \left(f_\beta - f_\beta^{eq} \right) + \delta_t \boldsymbol{F}_\alpha', \quad (1)$$

where f_α is the density distribution function, f_α^{eq} is its equilibrium distribution, t is the time, $\boldsymbol{x}$ is the spatial position, $\boldsymbol{e}$ is the discrete velocity along the αth direction, δ_t is the time step, $\boldsymbol{F}_\alpha'$ is the forcing term in the velocity space, and $\boldsymbol{M}$ is an orthogonal transformation matrix. $\boldsymbol{\Lambda}$ in Equation (1) is a diagonal matrix, and for D2Q9 lattice, $\boldsymbol{\Lambda}$ is given by

$$\boldsymbol{\Lambda} = diag \left(\tau_\rho^{-1}, \tau_e^{-1}, \tau_\zeta^{-1}, \tau_j^{-1}, \tau_q^{-1}, \tau_j^{-1}, \tau_q^{-1}, \tau_v^{-1}, \tau_v^{-1} \right). \quad (2)$$

Through the transformation matrix $\boldsymbol{M}$, $\boldsymbol{f}$ and $\boldsymbol{f}_\alpha^{eq}$ can be projected onto the moment space via $\boldsymbol{m} = \boldsymbol{M} \boldsymbol{f}$ and $\boldsymbol{m}^{eq} = \boldsymbol{M} \boldsymbol{f}^{eq}$, and the collision step of MRT LB equation (Equation (1)) can be rewritten as [25]

$$\boldsymbol{m}^* = \boldsymbol{m} - \boldsymbol{\Lambda} \left(\boldsymbol{m} - \boldsymbol{m}^{eq} \right) + \delta_t \left(\boldsymbol{I} - \frac{\boldsymbol{\Lambda}}{2} \right) \boldsymbol{S}, \quad (3)$$

where $\boldsymbol{I}$ is the unit tensor, and $\boldsymbol{S}$ is the forcing term in the moment space with $\left(\boldsymbol{I} - 0.5\boldsymbol{\Lambda} \right) \boldsymbol{S} = \boldsymbol{M} \boldsymbol{F}'$. For D2Q9 lattice, $\boldsymbol{m}^{eq}$ can be given by

$$\boldsymbol{m}^{eq} = \rho \left(1, -2 + 3|\boldsymbol{v}|^2, 1 - 3|\boldsymbol{v}|^2, v_x, -v_x, v_y, -v_y, v_x^2 - v_y^2, v_x v_y \right)^{\mathrm{T}}. \quad (4)$$

Here $\rho = \sum_\alpha f_\alpha$ is the macroscopic density, $\boldsymbol{v}$ is the macroscopic velocity which satisfies $|\boldsymbol{v}|^2 = v_x^2 + v_y^2$ and is calculated by

$$v = \frac{\sum_\alpha e_\alpha f_\alpha + 0.5\delta_t F}{\rho}, \tag{5}$$

where $F = (F_x, F_y)$ for two dimensional space is the force action on the fluid system. Then the streaming step of the MRT-LB equation can be formulated as

$$f_\alpha (x + e_\alpha \delta_t, t + \delta_t) = f_\alpha^* (x, t), \tag{6}$$

where $f^* = M^{-1} m^*$.

For the pseudopotential LB model in D2Q9 lattice case, the F in Equation (5) is given by

$$F = -G\psi(x) \sum_{\alpha=1}^{8} w_\alpha \psi(x + e_\alpha) e_\alpha, \tag{7}$$

where $\psi(x)$ is the interparticle potential, G is the interaction strength, and $w_{1,2,3,4} = 1/3$ and $w_{5,6,7,8} = 1/12$ are the weights. In the present work, the form of ψ proposed by Yuan *et al.* [27] is adopted which can be formulated as

$$\psi = \sqrt{\frac{2(p_{EOS} - \rho c_S^2)}{Gc^2}}, \tag{8}$$

where p_{EOS} is the pressure calculated by equation of state (EOS). The G in Equation (8) loses the meaning of the interaction strength and is used to ensure that the whole term inside the square root is positive [27]. The Carnahan-Starling (CS) EOS is adopted in the present work, which can be given by [27]

$$p_{EOS} = \rho RT \frac{1 + b\rho/4 + (b\rho/4)^2 - (b\rho/4)^3}{(1 - b\rho/4)^3} - a\rho^2, \tag{9}$$

where $a = 0.4963 R^2 T_c^2 / p_c$ and $b = 0.1873 RT_c / p_c$. Here T_c and p_c are the critical temperature and pressure, respectively.

F in Equation (7) can be incorporated in evolution equation via S with specific forcing scheme. Li *et al.* [25] proposed a MRT version forcing scheme to achieve thermodynamic consistency. For the D2Q9 lattice, Li's forcing scheme can be given by

$$S = \begin{pmatrix} 0 \\ 6(v_x F_x + v_y F_y) + \dfrac{0.75\varepsilon |F|^2}{\psi^2 \delta_t (\tau_e - 0.5)} \\ -6(v_x F_x + v_y F_y) - \dfrac{0.75\varepsilon |F|^2}{\psi^2 \delta_t (\tau_e - 0.5)} \\ F_x \\ -F_x \\ F_y \\ -F_y \\ 2(v_x F_x - v_y F_y) \\ v_x F_y + v_y F_x \end{pmatrix}, \tag{10}$$

where ε is a parameter related with the particle interaction range [28] and is proved by Li *et al.* to have the function of adjusting the thermodynamic consis-

tency [25]. Li's forcing scheme has the following advantages: a) maintaining a uniform layout with the a general form of the LB forcing scheme; b) achieving thermodynamic consistency only by tuning one constant parameter; and c) fully retaining the LBM's advantages of simple and efficient. In [21] it is found that the thermodynamic consistency is independent of kinematic viscosity for Li's improved forcing scheme, and the surface tension is independent of the relaxation time τ_v. These features make it more convenient to investigate the physical mechanism of the multiphase flows.

Unless otherwise specified, the unit adopted in this paper is the lattice unit of LBM, *i.e.* the units of the length, time, mass, velocity, density and pressure are *lu*(lattice unit), *ts*(time step), *mu*(mass unit), *mu lu*$^{-2}$, *lu ts*$^{-1}$ and *mu ts*$^{-2}$.

3. Cavitation Bubble Collapse near Rough Solid Wall

It is confirmed that the geometry is a crucial role on the process of the cavitation bubble collapse [29]. The interaction between collapse bubble and rough solid wall is a common issue abstracted from the cavitation applications involving the interactions between bubble and complex geometry boundary. In the present work, the rough solid wall is described by the wall with the geometries of periodic grooves with equal widths as shown in **Figure 1**. In this diagram, D_g and W_g are the depth and the width of groove, respectively. W_b is the width of bulge, and $W_P = W_g + W_b$ is the period width of the periodically arranged geometry.

The computational domain is shown in **Figure 2**. R_0, P_v and P_∞ are the initial radius, the pressure inside bubble and the ambient pressure, respectively. d_g and d_b are the distance from bubble center to groove bottom and bulge top, respectively. Based on the concept of the stand-off parameter [30], two non-dimensional parameters are introduced as follows to describe the positional relations between bubble and rough solid wall

$$\lambda_b = \frac{d_b}{R_0},\tag{11}$$
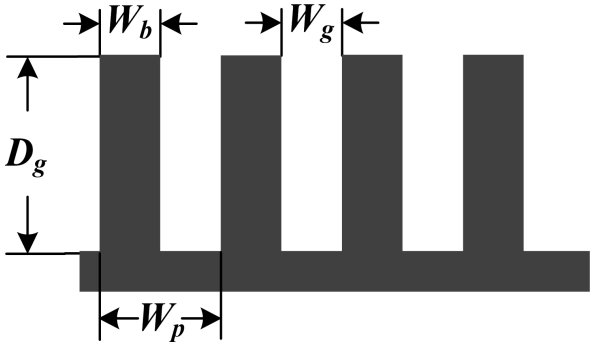
$$\lambda_g = \frac{d_g}{R_0}.\tag{12}$$

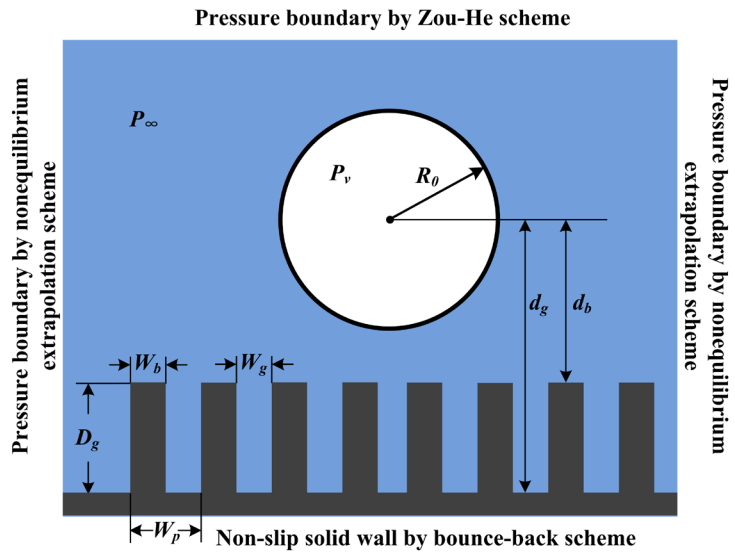**Figure 1.** Schematic diagram of rough wall geometry.

Figure 2. Computational domain for single solid wall case.

Here, λ_b, λ_g express the stand-off distances between bubble and bulge top, groove bottom, respectively.

The pressure boundary conditions, implemented by the nonequilibrium extrapolation scheme [31], are adopted in the directions of left and right. And, a constant pressure boundary condition is adopted in the top of computational domain by Zou-He scheme [32].

A 401×401 lattice is adopted in the simulations of this section. A vapor bubble with radius of $R = 80$ is initially placed at the center of the domain. The density field is initialized as [33]

$$\rho(x, y) = \frac{\rho_l + \rho_g}{2} + \frac{\rho_l - \rho_g}{2} \tanh\left(\frac{2\left(\sqrt{(x - x_0)^2 + (y - y_0)^2} - R_0 \right)}{W} \right), \quad (13)$$

where (x_0, y_0) is the center of the bubble, W is the prescribed width of the phase interface and is set as 5 in present work, $\tanh$ is the hyperbolic tangent function. The parameters of solid wall geometry are set as $D_g = 144$, $W_b = W_g = 10$, $W_p = 20$, $d_g = 160$ and $d_b = 15$, respectively.

The parameters for the present MRT pseudopotential LB model are chosen as follows: $\tau_\rho^{-1} = \tau_j^{-1} = 1.0$, $\tau_e^{-1} = \tau_\zeta^{-1} = 1.0$, $\tau_q^{-1} = 1.1$, $\tau_v = 0.6$ and $\varepsilon = 1.86$. For CS EOS, $a = 0.5$, $b = 4$ and $R = 1$. The temperature $T = 0.7T_c$. In order to simulate the bubble collapse process, a positive pressure difference $\Delta P = P_\infty - P_v$ is achieved by artificially tuning the initial liquid density based on the equilibrium state. In this section, the pressure difference is $\Delta P = 0.0116$.

4. Results

4.1. Evolution of Density Field

The evolution of density field is shown in **Figure 3**. The deformation of bubble profile can be investigated from density field. The initial spherical bubble begins
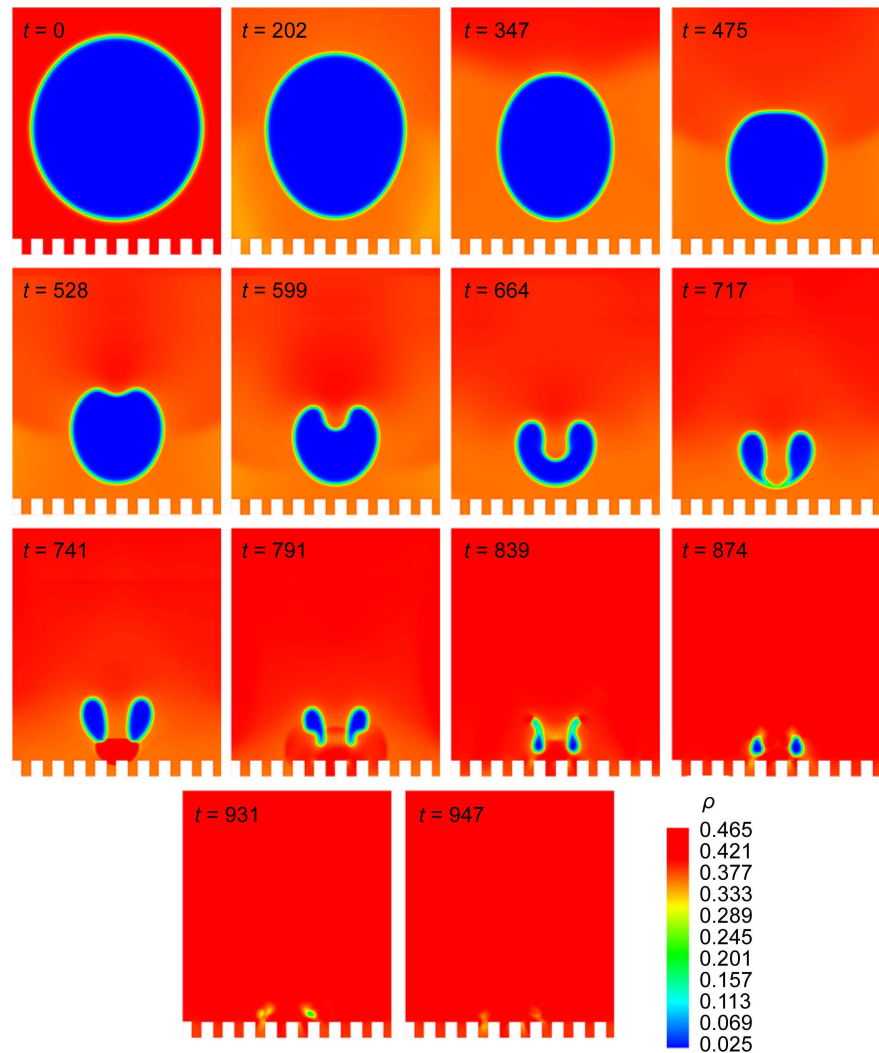
Figure 3. Density field evolution of the collapsing bubble near rough solid wall.

to collapse motivated by the pressure difference from $t = 0$. The velocity of collapse is slow at the starting stage. Until $t = 202$, the bubble profile appears obvious deformation, *i.e.*, the radius of curvature reduce towards the rough solid wall. Then, the bubble becomes an ellipsoid and the density just over the bubble increases. Along with the diffusion of the higher density area, the top of the bubble is flatten, and then concaved directing the solid wall. At the same time, the more dense and concentrated density area appears at the concave and accelerate the shift of the bubble profile. As a result, the jet is formed. The first collapse happens when the upper bubble wall clashes the bottom wall. The jet perforates the bottom wall and produces a crucial bubble. The shock wave generated by the first collapse propagates rapidly towards the rough solid wall and bounce back. The bubble experiences the complex and volatile deformation at the last stage under the jet which includes shock wave and bounce wave.

Figure 3 describes the whole process of bubble collapse with time *t*. Comparing with the flat solid wall case, the bubble collapse near rough solid wall appears the similar dynamics process [20]. The differences are mainly reflected in two

aspects. The first one is the bounce of the shock wave in rough solid wall case is weaker than the one in the planar wall case. The strength and the reflection path of the shock wave are affected by the geometry of the rough solid wall. The second one is the geometry of the rough solid wall affects the bubble deformation, especially at the last stage. In order to be more intuitive, pressure field evolution of the collapsing bubble is investigated in the next section.

4.2. Evolution of Pressure and Velocity Field

Several representative moments of the pressure and velocity evolution are shown in **Figure 4**. At $t = 528$, one high pressure area emerges at the concave of bubble top. It is consistent with the analysis of the density distribution at the same moment. At the same time, the fluid velocity is increased towards the solid wall which formats the inceptive jet. The jet velocity at the concave is significantly higher than that of other areas in the moment. Along with the sagging of the upper bubble wall, the jet velocity is higher and higher. At $t = 717$, the first collapse occurs. The clash between the upper and the bottom walls induces shock wave as shown in $t = 741$. And at the same moment, the bubble is broken by the high velocity jet. Affected by the vortexes, which are induced by the jet and the bouncing back shock wave, the crucial bubble deforms and then collapses close to the rough solid wall. From **Figure 4**, we can find that the shock waves bounce intensively at the solid surfaces of the bulges top, and propagate unceasingly into the grooves with decreasing strength. The fluid jet follows the similar mode. It is inevitable that the shock wave and the jet will erode and impact the rough solid wall.
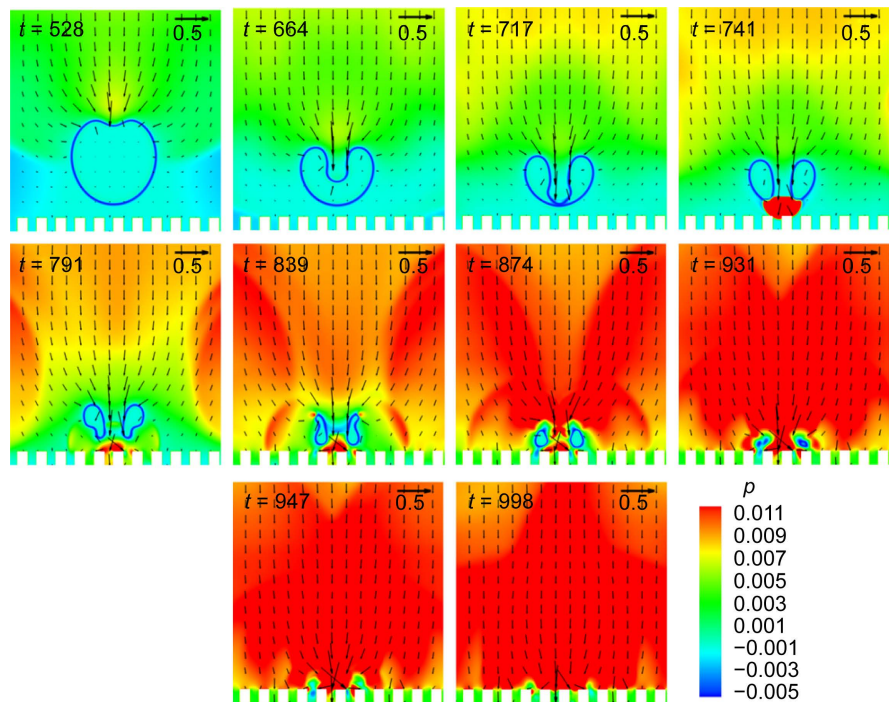

Figure 4. Pressure and velocity field evolution of the collapsing bubble near rough solid wall.

Figure 5 gives the finer detail display of the interaction between the pressure, velocity and the rough solid wall at $t = 998$. It is found that in the groove and near the bulge, which are off-center the collapse position, the vortexes are formed. Conversely, the laminar flows are formed in the groove just under the collapse position. The vortexes and the laminar flows induce the remarkable eroding effect on the solid surface of the bulge and the groove, respectively.

4.3. Analysis of Eroding Effect

In order to investigate the eroding process and effect induced by bubble collapse close to the rough solid wall, four test sections are set at the bulges top and the grooves side walls as shown in Figure 5. The coordinates of these four test sections are $(a \mid x = 191, y \in [257, 270])$, $(b \mid x = 211, y \in [257, 270])$, $(c \mid y = 256, x \in [200, 210])$ and $(d \mid y = 256, x \in [220, 230])$, respectively. The pressure evolution and the velocity evolution of these four test sections, from 730 ts to 1000 ts, are displayed in Figure 6 and Figure 7.

Form Figure 6, we can find that the test section *a* experiences three pressure peaks during the time interval of observation. The closer to the groove entrance, the greater the pressure amplitude is. The first pressure peak with the greatest amplitude is the result of shock wave. The second is the water hummer effect of jet. However, as the test section is parallel with jet direction, the pressure amplitude is weaker than the first pressure peak. The third pressure peak is induced by the second collapse. The pressure evolution at the test section *b* displays similar pattern. Due to the impeding effect of the bulge, the lower pressure area is induced near the test section *b*. The test section *c* is just under the collapse position, so the three pressure peaks are greater than the test section *a* and *b*. The pressure pattern of the test section *d* is similar as that of *b* on account of the larger deviation
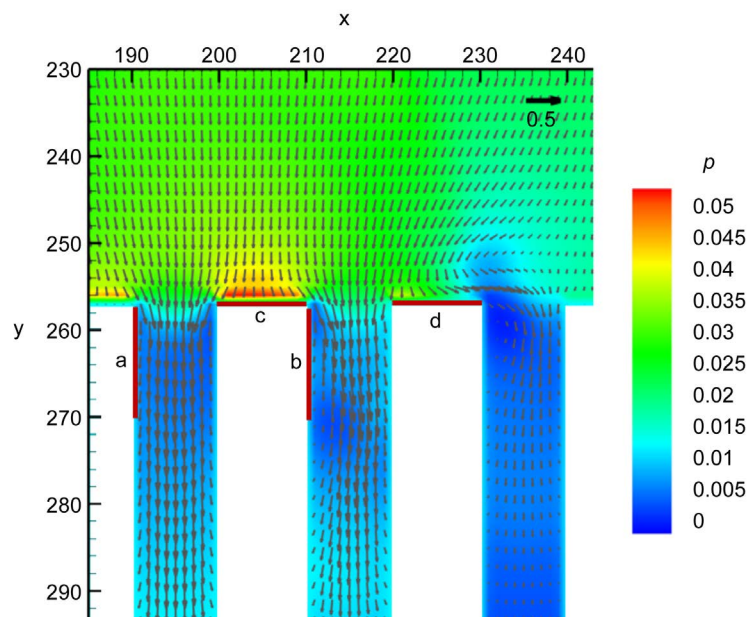

Figure 5. Pressure and velocity distribution at rough solid wall after the bubble collapse.
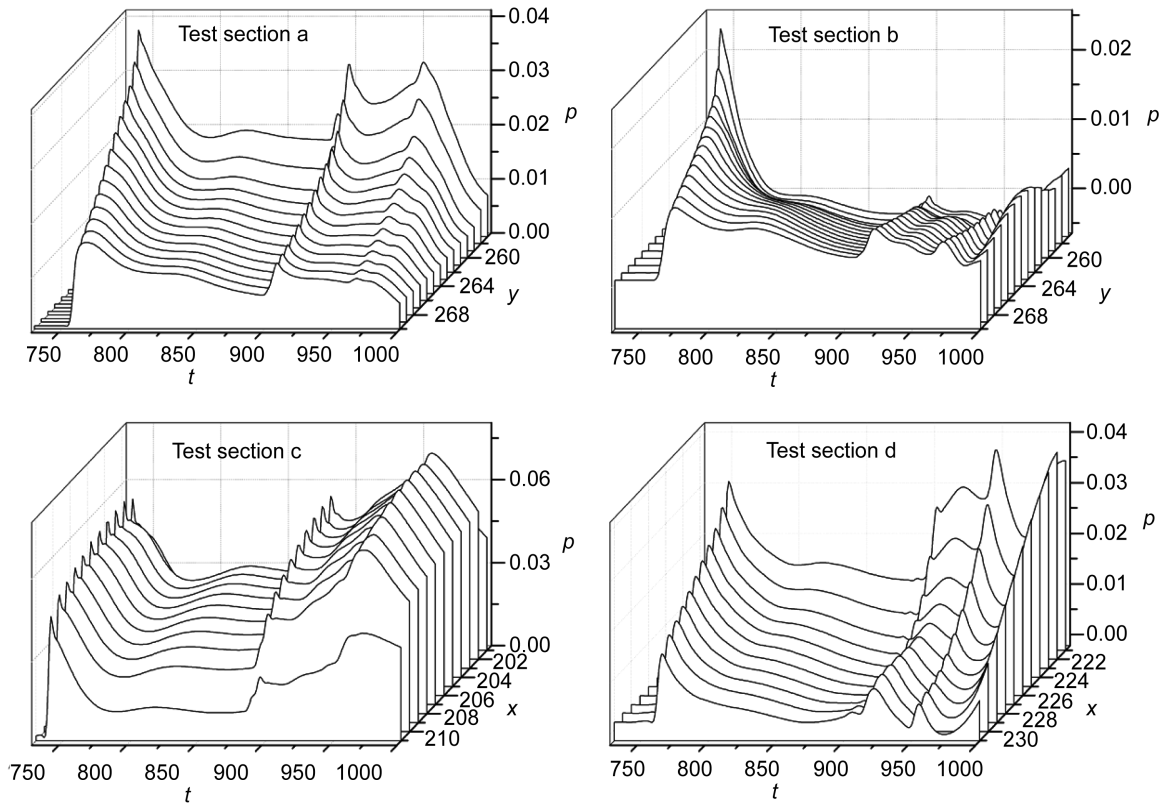
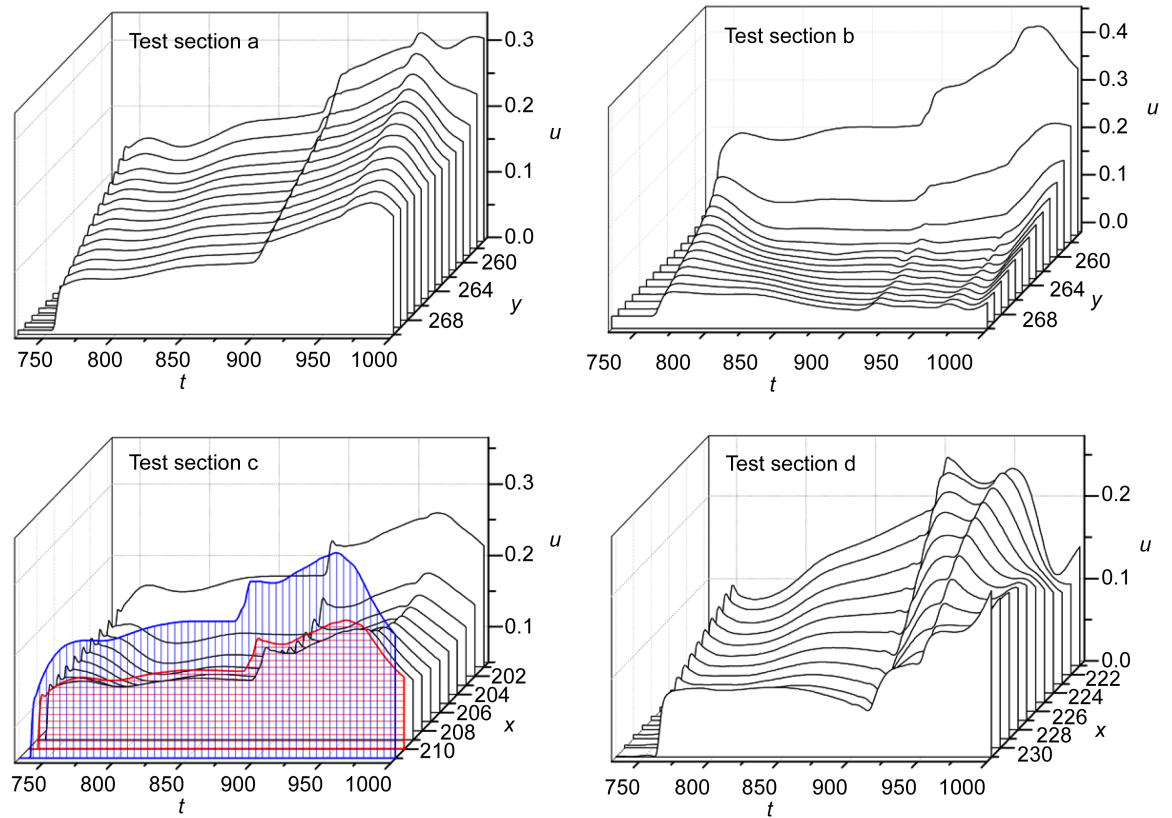**Figure 6.** Pressure evolution at the test sections.

Figure 7. Velocity evolution at the test sections.

from the collapse station. But the pressure amplitudes are higher than the test section *b* because of the closer distance from the solid wall. The pressure evolution at the four test sections demonstrates that no matter the bulge solid wall or the groove entrance experience the oscillation of pressure.

The velocity evolution of the four test sections are shown in Figure 7. For the test section *a*, every test point experiences the similar process of the fluid velocity, which increases sharply and then gradually rises to the peak. The pattern of the velocity is same as the pressure, *i.e.*, the closer to the groove entrance, the greater the velocity is. It demonstrated that the groove geometry impedes both of the pressure and the velocity at the groove side walls. Although the same near the entrance, the test section *b* shows a different pattern. Under the combined action of shock wave and jet, the vortexes are induced at *b*. The velocity evolution pattern of the test section *c* is symmetric in *x* direction. Due to the non-slid effect of solid wall, the fluid velocity at center of the bulge is lower than the sides, which are closer to the groove entrances. For the test section *d*, the velocity pattern is more diversified with lower fluid velocity than other test sections. The oscillation of velocity is more violent for farther distance from collapse position. The last velocity peaks are related with the collapse of the crucial bubble.

In summary, the eroding effect at the solid wall of the bulge part is weaker than that at the side walls, and is more obvious at the side walls of the grooves than other sections. From the pressure and velocity evolution patterns, it demonstrates that the fluid velocity accounts for the eroding effect at the side walls of the grooves, and the pressure accounts for the eroding effect at the bulge part of the rough solid wall.

5. Conclusions

For the modeling of the collapsing bubble near rough solid wall, an improved MRT pseudopotential LB model was adopted with the modified forcing scheme by Li *et al.* Then the bubble collapse near rough solid wall was simulated. The bubble collapse mechanism was investigated from the dynamic process including bubble profiles evolution, pressure and velocity field evolution. The eroding effects of shock wave and jet were analyzed in details. It is found that the process and the effect of bubble collapse are affect seriously by the geometry of solid boundary. In the present work, the interaction between the collapsing bubble and the geometries boundary structured with periodic grooves was investigated. We found that the fluid velocity is the major cause for the eroding effect at the side walls of the grooves, and the pressure is the major cause for the eroding effect at the bulge part of the rough solid wall.

The improved forcing scheme proposed by Li *et al.* provides a convenient and efficient approach to achieve thermodynamic consistency. By the modelling of the bubble collapse near the rough solid wall, it is demonstrated that the MRT pseudopotential LB model improved by the modified forcing scheme has enough stability to describe the whole process of bubble collapse and the interaction between the collapsing bubble and complex geometry boundary.

References

[1] Abboud, J.E. and Oweis, G.F. (2013) Themicrojetting Behavior from Single Laser-Induced Bubbles Generated above a Solid Boundary with a Through Hole. *Experiments in Fluids*, **54**, 1438. https://doi.org/10.1007/s00348-012-1438-6

[2] Hashmi, A., Yu, G., Reilly-Collette, M., Heiman, G. and Xu, J. (2012) Oscillating Bubbles: A Versatile Tool for Lab on a Chip Applications. *Lab on a Chip*, **12**, 4216-4227. https://doi.org/10.1039/c2lc40424a

[3] Naudé, C.F. and Ellis, A.T. (1961) On the Mechanism of Cavitation Damage by Nonhemispherical Cavities Collapsing in Contact with a Solid Boundary. *Journal of Basic Engineering*, **83**, 648-656. https://doi.org/10.1115/1.3662286

[4] Li, B.B., Jia, W., Zhang, H.C. and Lu, J. (2014) Investigation on the Collapse Behavior of a Cavitation Bubble near a Conical Rigid Boundary. *Shock Waves*, **24**, 317-324. https://doi.org/10.1007/s00193-013-0482-3

[5] Aganin, A.A., Ilgamov, M.A., Kosolapova, L.A. and Malakhov, V.G. (2016) Dynamics of a Cavitation Bubble near a Solid Wall. *Thermophysics and Aeromechanics*, **23**, 211-220. https://doi.org/10.1134/S0869864316020074

[6] Magaletti, F., Gallo, M., Marino, L. and Casciola, C.M. (2016) Shock-Induced Collapse of a Vapor Nanobubble near Solid Boundaries. *International Journal of Multiphase Flow*, **84**, 34-45. https://doi.org/10.1016/j.ijmultiphaseflow.2016.02.012

[7] Hsu, C.Y., Liang, C.C., Nguyen, A.T. and Teng, T.L. (2014) A Numerical Study on the Underwater Explosion Bubble Pulsation and the Collapse Process. *Ocean Engineering*, **81**, 29-38. https://doi.org/10.1016/j.oceaneng.2014.02.018

[8] Zhang, A.M. and Liu, Y.L. (2015) Improved Three-Dimensional Bubble Dynamics Model Based on Boundary Element Method. *Journal of Computational Physics*, **294**, 208-223. https://doi.org/10.1016/j.jcp.2015.03.049

[9] Chen, S. and Doolen, G.D. (1998) Lattice Boltzmann Method for Fluid Flows. *Annual Review of Fluid Mechanics*, **30**, 329-364. https://doi.org/10.1146/annurev.fluid.30.1.329

[10] Succi, S. (2001) The Lattice Boltzmann Equation: For Fluid Dynamics and Beyond. Oxford University Press, Oxford.

[11] Gunstensen, A.K., Rothman, D.H., Zaleski, S. and Zanetti, G. (1991) Lattice Boltzmann Model of Immiscible Fluids. *Physical Review A*, **43**, 4320. https://doi.org/10.1103/physreva.43.4320

[12] Shan, X. and Chen, H. (1993) Lattice Boltzmann Model for Simulating Flows with Multiple Phases and Components. *Physical Review E*, **47**, 1815. https://doi.org/10.1103/physreve.47.1815

[13] Shan, X. and Chen, H. (1994) Simulation of Non Ideal Gases and Liquid-Gas Phase Transitions by the Lattice Boltzmann Equation. *Physical Review E*, **49**, 2941. https://doi.org/10.1103/physreve.49.2941

[14] Swift, M.R., Osborn, W.R. and Yeomans, J.M. (1995) Lattice Boltzmann Simulation of Non-Ideal Fluids. *Physical Review Letters*, **75**, 830. https://doi.org/10.1103/physrevlett.75.830

Scientific Research Publishing

[15] Chen, L., Kang, Q., Mu, Y., He, Y.L. and Tao, W.Q. (2014) A Critical Review of the Pseudo Potential Multiphase Lattice Boltzmann Model: Methods and Applications. *International Journal of Heat and Mass Transfer*, **76**, 210-236.

[16] Huang, H., Sukop, M. and Lu, X. (2015) Multiphase Lattice Boltzmann Methods: Theory and Application. John Wiley & Sons Ltd., Chichester.
https://doi.org/10.1002/9781118971451

[17] Sukop, M.C. and Or, D. (2005) Lattice Boltzmann Method for Homogeneous and Heterogeneous Cavitation. *Physical Review E*, **71**, Article ID: 046703.
https://doi.org/10.1103/physreve.71.046703

[18] Chen, X.P., Zhong, C.W. and Yuan, X.L. (2011) Lattice Boltzmann Simulation of Cavitating Bubble Growth with Large Density Ratio. *Computers & Mathematics with Applications*, **61**, 3577-3584.

[19] Mishra, S.K., Deymier, P.A., Muralidharan, K., Frantziskonis, G., Pannala, S. and Simunovic, S. (2010) Modeling the Coupling of Reaction Kinetics and Hydrodynamics in a Collapsing Cavity. *Ultrasonics Sonochemistry*, **17**, 258-265.

[20] Shan, M.L., Zhu, C.P., Xi, Z.H.O.U., Cheng, Y.I.N. and Han, Q.B. (2016) Investigation of Cavitation Bubble Collapse near Rigid Boundary by Lattice Boltzmann Method. *Journal of Hydrodynamics*, **28**, 442-450.

[21] Shan, M.L., Zhu, C.P., Yao, C., Yin, C. and Jiang, X.Y. (2016) Pseudopotential Multi-Relaxation-Time Lattice Boltzmann Model for Cavitation Bubble Collapse with High Density Ratio. *Chinese Physics B*, **25**, Article ID: 104701.
https://doi.org/10.1088/1674-1056/25/10/104701

[22] Li, Q. and Luo, K.H. (2014) Thermodynamic Consistency of the Pseudopotential Lattice Boltzmann Model for Simulating Liquid-Vapor Flows. *Applied Thermal Engineering*, **72**, 56-61.

[23] Kupershtokh, A.L., Medvedev, D.A. andKarpov, D.I. (2009) On Equations of State in a Lattice Boltzmann Method. *Computers & Mathematics with Applications*, **58**, 965-974.

[24] Li, Q., Luo, K.H. and Li, X.J. (2012) Forcing Scheme in Pseudopotential Lattice Boltzmann Model for Multiphase Flows. *Physical Review E*, **86**, Article ID: 016709.
https://doi.org/10.1103/physreve.86.016709

[25] Li, Q., Luo, K.H. and Li, X.J. (2013) Lattice Boltzmann Modeling of Multiphase Flows at Large Density Ratio with an Improved Pseudopotential Model. *Physical Review E*, **87**, Article ID: 053301. https://doi.org/10.1103/physreve.87.053301

[26] Li, Q., Luo, K.H., Kang, Q.J., He, Y.L., Chen, Q. and Liu, Q. (2016) Lattice Boltzmann Methods for Multiphase Flow and Phase-Change Heat Transfer. *Progress in Energy and Combustion Science*, **52**, 62-105.

[27] Yuan, P. and Schaefer, L. (2006) Equations of State in a Lattice Boltzmann Model. *Physics of Fluids*, **18**, Article ID: 042101. https://doi.org/10.1063/1.2187070

[28] Shan, X. (2008) Pressure Tensor Calculation in a Class of Nonideal Gas Lattice Boltzmann Models. *Physical Review E*, **77**, Article ID: 066702.
https://doi.org/10.1103/physreve.77.066702

[29] Shi, D.Y., Wang, Z.K. and Zhang, A.M. (2014) Study on Coupling Characteristics between Bubble and Complex Walls at the Same Scale. *Acta Physica Sinica*, **63**, 533-538.

[30] Plesset, M.S. and Chapman, R.B. (1971) Collapse of an Initially Spherical Vapour Cavity in the Neighbourhood of a Solid Boundary. *Journal of Fluid Mechanics*, **47**, 283-290. https://doi.org/10.1017/S0022112071001058

[31] Guo, Z.-L., Zheng, C.-G. and Shi, B.-C. (2002) Non-Equilibrium Extrapolation Me-

thod for Velocity and Pressure Boundary Conditions in the Lattice Boltzmann Method. *Chinese Physics*, **11**, 366. https://doi.org/10.1088/1009-1963/11/4/310

[32] Zou, Q. and He, X. (1997) On Pressure and Velocity Boundary Conditions for the Lattice Boltzmann BGK Model. *Physics of Fluids*, **9**, 1591-1598. https://doi.org/10.1063/1.869307

[33] Huang, H., Krafczyk, M. and Lu, X. (2011) Forcing Term in Single-Phase and Shan-Chen-Type Multiphase Lattice Boltzmann Models. *Physical Review E*, **84**, Article ID: 046710. https://doi.org/10.1103/physreve.84.046710